tic. The large initial weakening and reintensification of the THC appear to be induced by the massive, initial infusion of fresh, low density water and its abrupt termination, respectively. After the initial fluctuation, the THC reintensifies gradually (Fig. 1*b*), increasing both SST and SSS during the next few hundred years. The damped oscillation of the THC, which occurs during the reintensification, resembles the weaker oscillation which Delworth *et al.*[10] found in the control experiment. The structures of the THC at the beginning, shortly after the termination of the freshwater infusion, and at the end of the experiment are illustrated and discussed in Fig. 4. and its legend.

The coupled model produced large and rapid changes in surface air temperature and the rate of deep-water formation reminiscent of those inferred from the palaeoceanographic[4,11] and ice-core records[1,2]. But during the glacial and postglacial periods, one can identify many cold episodes of low ice-core $\delta^{18}O$ which last much longer than the simulated period of low SST in the present FW experiment. Obviously, the cold period could last longer if a meltwater flux of smaller magnitude were applied much longer than 10 years, or a massive armada of icebergs was discharged and melted in the middle of the cold period[12]. Both of these mechanisms, which release the fresh water with low $\delta^{18}O$, could have operated during the cold event of 14,500 ^{14}C-years ago, accounting for the $\delta^{18}O$ minimum in planktonic foraminifera noted by Keigwin and Lehman[13]. On the other hand, the total amount of melt water infused around the beginning of the Younger Dryas event might have been substantially larger than that imposed in the present experiment[9]. If so, the THC could be weakened enough to keep it at a reduced intensity despite the relatively small supply of fresh water during most of the cold Younger Dryas period. It is likely that the rate of meltwater supply during the Younger Dryas was too small to reverse the positive $\delta^{18}O$ anomaly associated with low SST, yielding the planktonic $\delta^{18}O$ maximum noted by Keigwin and Lehman[13].

By use of a coupled ocean–atmosphere model, Manabe and Stouffer[14] obtained two stable equilibria, that is, active and inactive modes of the THC in the Atlantic Ocean. They suggested that the inactive mode resembles the oceanic state of Younger Dryas. However, the palaeoceanographic evidence[15] indicates not only a markedly reduced deep-water formation but also a significant ventilation of the upper ocean layer during the cold period. It is therefore likely that the transient state of weak and shallow THC encountered during the present FW experiment is more consistent with the palaeoceanographic signatures of Younger Dryas than the inactive equilibrium mentioned above. The freshwater-induced transitions among multiple equilibria of a simple coupled model were examined, for example, by Stocker *et al.*[16] and Rahnstorf[21].

The evolutions of the THC and SST, which were recently obtained by Rahmstorf[17] by use of his coupled model with a highly simplified atmosphere and idealized geography, and without the seasonal variation, is quite different from those described in the present study. His simulation shows that, in response to an infusion of fresh water, the THC rapidly weakens but restores its original intensity very quickly, leaving behind an equilibrium state of shallow convection and cold surface water. In the coupled model used here, it is not possible to sustain such shallow convection indefinitely at a given grid point, because it is influenced by the noisy and seasonally varying atmosphere.

The recent study of Manabe and Stouffer[18,19] reveals that, associated with the CO_2-induced warming of the model atmosphere, the poleward transport of water vapour increases, causing marked increases in precipitation, and accordingly, freshwater supply in the high latitudes. The simulated multi-century response of the THC to the doubling of atmospheric CO_2 (refs 18, 19) resembles the response to the freshwater input described here. Thus substantial changes in the intensity and distribution of the THC could also occur in response to future increases of greenhouse gases in the atmosphere. □

Received 30 May; accepted 3 October 1995.

1. Dansgaard, W. *et al. Science* **218,** 1273–1277 (1982).
2. Johnsen, S. J. *et al. Nature* **359,** 311–313 (1992).
3. Broecker, W. S. *Paleoceanography* **5,** 459–467 (1990).
4. Keigwin, L. D. & Jones, G. A. *J. geophys. Res.* **99,** 12397–12410 (1994).
5. Stouffer, R. J., Manabe, S. & Bryan, K. *Nature* **342,** 660–662 (1989).
6. Manabe, S., Stouffer, R. J., Spelman, M. J. & Bryan, K. *J. Clim.* **4,** 785–818 (1991).
7. Stouffer, R. J., Manabe, S. & Vinnikov, K. Ya. *Nature* **367,** 634–636 (1994).
8. Marotzke, J. & Stone, P. *J. phys. Oceanogr.* **25,** 1350–1364 (1995).
9. Fairbanks, R. G. *Nature* **342,** 637–642 (1989).
10. Delworth, T., Manabe, S. & Stouffer, R. J. *J. Clim.* **6,** 1993–2011 (1993).
11. Boyle, E. A. & Rosener, P. *Paleogeogr. Paleoclimatol. Paleoecol.* **89,** 113–124 (1990).
12. Bond, G. *et al. Nature* **365,** 143–147 (1993).
13. Keigwin, L. D. & Lehman, S. *Paleoceanography* **9,** 185–194 (1994).
14. Manabe, S. & Stouffer, R. J. *J. Clim.* **1,** 841–866 (1988).
15. Boyle, E. A. & Keigwin, L. *Nature* **330,** 35–40 (1987).
16. Stocker, T. F., Wright, D. G. & Mysak, L. A. *J. Clim.* **5,** 773–797 (1992).
17. Rahmstorf, S. *Nature* **372,** 82–85 (1994).
18. Manabe, S. & Stouffer, R. J. *Nature* **364,** 215–218 (1993).
19. Manabe, S. & Stouffer, R. J. *Clim.* **7,** 5–23 (1994).
20. Wright, D. G. & Stocker, T. F. *J. phys. Oceanogr.* **21,** 1713–1724 (1991).
21. Rahnstorf, S. *Nature* **378,** 145–149 (1995).

ACKNOWLEDGEMENTS. We thank A. J. Broccoli, T. L. Delworth, S. Griffies, L. D. Keigwin, J. D. Mahlman and J. Miller who offered valuable comments for improving the manuscript.

Plate boundary reorganization at a large-offset, rapidly propagating rift

R. N. Hey*, P. D. Johnson*, F. Martinez*, J. Korenaga†, M. L. Somers‡, Q. J. Huggett‡, T. P. LeBas‡, R. I. Rusby‡ & D. F. Naar§

* Hawaii Institute of Geophysics and Planetology, School of Ocean and Earth Science and Technology, University of Hawaii, Honolulu, Hawaii 96822, USA
† MIT/WHOI Joint Program, Woods Hole Oceanographic Institution, Woods Hole, Massachusetts 02543, USA
‡ Institute of Oceanographic Sciences, Wormley, Godalming GU8 5UB, UK
§ Department of Marine Science, University of South Florida, St Petersburg, Florida 33701, USA

THE existence of rapidly spinning microplates along the southern East Pacific Rise has been documented by geophysical swath-mapping surveys[1–6], and their evolution has been successfully described by an edge-driven kinematic model[7]. But the mechanism by which such microplates originate remains unknown. Proposed mechanisms[1–10] have generally involved rift propagation[11], possibly driven by hotspots or changes in direction of sea-floor spreading. Here we present geophysical data collected over the Earth's fastest spreading centre, the Pacific–Nazca ridge between the Easter and Juan Fernandez microplates (Fig. 1), which reveal a large-offset propagating rift presently reorganizing the plate boundary geometry. A recent episode of rapid 'duelling' propagation of the historically failing spreading centre in this system has created a 120 × 120 km overlap zone between dual active spreading centres, which may be the initial stage of formation of a new microplate.

The dual spreading centres, shown by shallow ridges and acoustically reflective sea floor, overlap between about 28.5°–29.5° S, 113°–112° W (Figs 2, 3). The West ridge has been propagating south[3,12] for ~1.5 Myr, transferring young Pacific lithosphere to the Nazca plate (shown by the rotated fabric extending northeast from the overlap zone). It is the shallowest part of the entire East Pacific Rise, reaching above 2,100 m. It is also the most highly inflated, defined by cross-sectional area above the average 0.5 Myr depth[30], reaching nearly 9 km^2. This propagator has created a shallow V-shaped area bounded by pseudofaults[11] which indicate a steady propagation rate nearly equal to the spreading rate, ~135 km Myr^{-1}. The characteristic parabolic propagator tip results from the acceleration from no spreading to the full rate[13,14]. Spreading along most of the West ridge

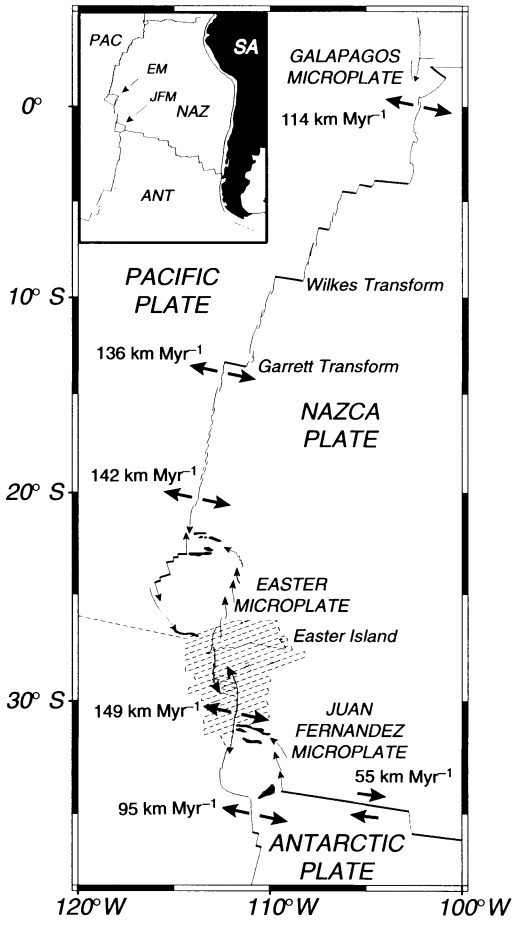

FIG. 1 Location map modified from refs 6 and 28. Light lines are ridges, those with arrows are propagating. Heavy straight lines are transform faults. Spreading rates are from ref. 16, modified by the revised age of 0.78 Myr for the Brunhes/Matuyama reversal[17].

segments has been highly asymmetric, with recent accretion rates on segment W2 ~5 times higher to the east than west (Fig. 3), suggesting multiple unresolved rapid propagation events[13,15]. The recent spreading rate here is significantly lower than the 150 km Myr^{-1} observed on the eastern system and predicted[16] for Pacific–Nazca opening (these rates use the revised astronomically calibrated timescale[17] which gives rates ~6% slower than recently thought). This crustal deficit was mostly taken up by spreading on the failing rifts during episodes of duelling propagation.

The East ridge away from the tip is also shallow and unusually flat (2,350 ± 20 m) despite large variations in inflation. Although it has been the failing rift in this propagating rift system, a narrow V-shaped area of highly reflective shallow sea floor cutting through older less-reflective, transferred lithosphere (Fig. 2*b*) indicates that it has propagated north recently[18], creating an ~15,000 km^2 overlap zone. Duelling propagation has been recognized elsewhere[19–22] on much smaller scales and attributed to competing magma sources[20,21].

The 1:1 aspect ratio of the overlap zone is similar to those of the Easter[1–3] and Juan Fernandez[4–6] microplates and large propagator systems[23] rather than the 3:1 ratio characteristic of overlapping spreading centres[20,21]. The southern boundary of this zone is marked by a narrow linear ridge (Fig. 2*a*) trending ~110°; no localized boundary structure is seen in the north. This boundary does not at present intersect the East ridge axis but ends at what we interpret as an inner pseudofault produced by East ridge propagation ~0.2 Myr ago, indicating a minimum northward propagation velocity of ~600 km Myr^{-1}. Most of the overlap zone is characterized by northeast-trending structures similar to the oblique structures found in the Galapagos 95.5° W propagator shear zone and interpreted there as resulting from 'bookshelf' faulting[23]. Fault plane solutions (Fig. 3) for this area are consistent with bookshelf faulting[24], as is shipboard three-component magnetometer vector analysis[25]. Most of the earthquakes occur in the inner pseudofault zones of the duelling propagators. The southeastern part of the overlap zone shows much lower reflectivity than the rest (Fig. 2*b*), indicating a piece of older Pacific lithosphere transferred into this zone by the southward propagation of the West rift. This area is also relatively shallow, suggesting that lithospheric transfer here involves compression or possibly seamount formation.

Despite the preponderance of northeast-trending structures in the overlap zone, there are two northwest-trending structures near the southern margin (Figs 2, 3). The deep (~3,500 m) graben trending ~135° near 29.5° S, 112.5° W resembles rift structures mapped in Afar (P. Tapponnier and I. Manighetti, personal communication) and is probably a current axis of tectonic rifting with slow spreading (D. McKenzie, personal communication). The narrow scarp just east of this graben forms the southwestern margin of the old lithosphere in the overlap zone and extends into the southern boundary zone. Because of the age asymmetry across this scarp, it is different from the structures identified as failed rifts.

The failed rifts northeast of this area are evident in the side-scan reflectivity and structural data (Figs 2, 3) as relatively young areas of high reflectivity and northwest-trending structures cutting into the relatively older zone of transferred lithosphere (fossil overlap zone). The failed rift tips line up along a trend of ~033°, in good agreement with the 029° trend predicted by theoretical equations[14,26] for rift propagation. Some of these failed rifts are deep grabens, typical of several propagator systems[26]. Others are bathymetric highs which more closely resemble the abandoned ridges on the 20.8° S duelling propagator system[20].

There appear to have been about six previous major failed rifts left behind on the Nazca plate, with the (now) northward-propagating East rift segment E1 destined to be the next in this series (Fig. 3) unless a new microplate forms here. Although they penetrate 50–100 km into the zone of transferred lithosphere, the rift widths are typically less than 10 km, with the widest (other than E1) ~30 km wide. Although spreading must slow on these features as they fail, which probably explains why many are grabens[26], this still suggests very short spreading histories at these locations. The general lack of major changes in trend of the transferred sea-floor fabric across the failed rifts is evidence that they failed rapidly following episodes of 'superfast' propagation or ridge jumps, very similar to those modelled as cyclical ridge jumps in the Juan de Fuca area[22]. The spacing of the failed rifts suggests an irregular episodicity of ~0.3 Myr. The series of failed rifts appears to be bounded to the northeast by the western part of the SOEST fracture zone (Figs 2, 3), although some rifts seem to have propagated slightly north of this fracture zone just before failing.

Figure 4 shows the hypothesized schematic evolution of this area from a stable dextral Pacific–Nazca transform fault south of the Easter microplate, to a giant propagator system with episodic duelling propagation of the failing rift, to its present configuration. At ~1.5 Myr the dominant southward propagation began, as well as contemporaneous northward propagation[1,3,12] away from this same shallow area. The change in trend of the SOEST fracture zone suggests a clockwise rotation of Pacific–Nazca motion at that time. These propagating segments (shown in Fig. 4 by the diamond-shaped pseudofault pattern) are the shallowest of the entire East Pacific Rise system, suggesting that they are probably driven both to north and south by increased magma supply[12,13] (probably from the nearby Easter hotspot) and the resulting gravitational spreading

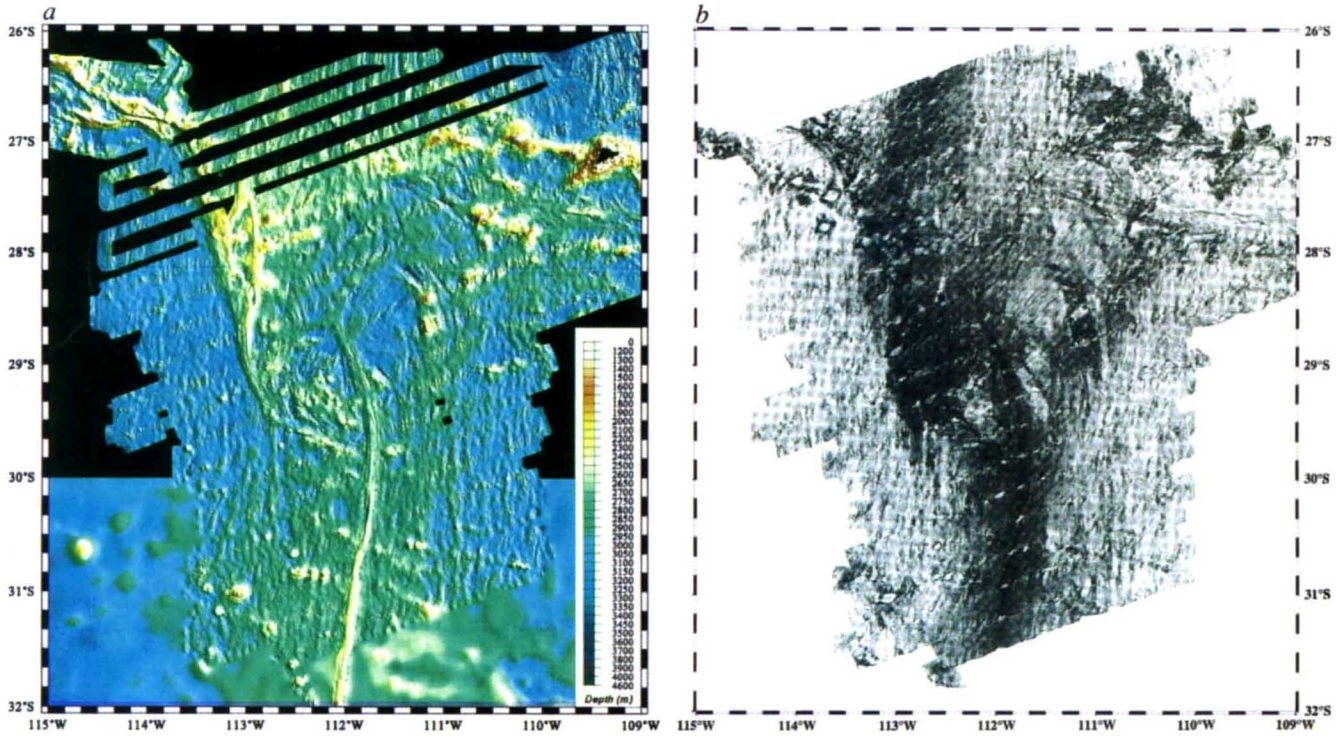

FIG. 2 *a*, Colour-shaded bathymetric relief map, illuminated from the northeast. High-resolution 10-km-wide SeaBeam 2000 bathymetric swaths are overlaid onto the wider (24 km) GLORI-B swaths. This was the first expedition in which this modified GLORIA system collected swath bathymetry. The southwestern margin of the Easter microplate is digitized from hand-contoured SeaMARC II data[3]. The regional data south of 30° S are derived from satellite altimetry data[29]. *b*, GLORI-B sidescan sonar mosaic. Strong acoustic backscatter returns (usually associated with recent volcanism or rough surfaces) are shown dark, weak backscatter areas (usually associated with sedimented areas or shadow zones) are white. Data have been digitally processed to correct for geometrical distortions and to equalize the gain at different ranges.

stresses[27]. The propagation is facilitated by increased driving forces and decreased resistive forces[27] at these 'superfast' spreading rates. All ridges presently spreading faster than 142 km Myr^{-1} (Fig. 1) are being reorganized by rift propagation[28].

Is this overlapping system a microplate or a propagator? The clear history of failed rift tips suggests the latter. Also, the NE structural trends within the overlap zone (Figs 2, 3) are consistent with the maximum rotation of 42° predicted by the propagating rift equations[14,26]. If the overlap zone were behaving as a

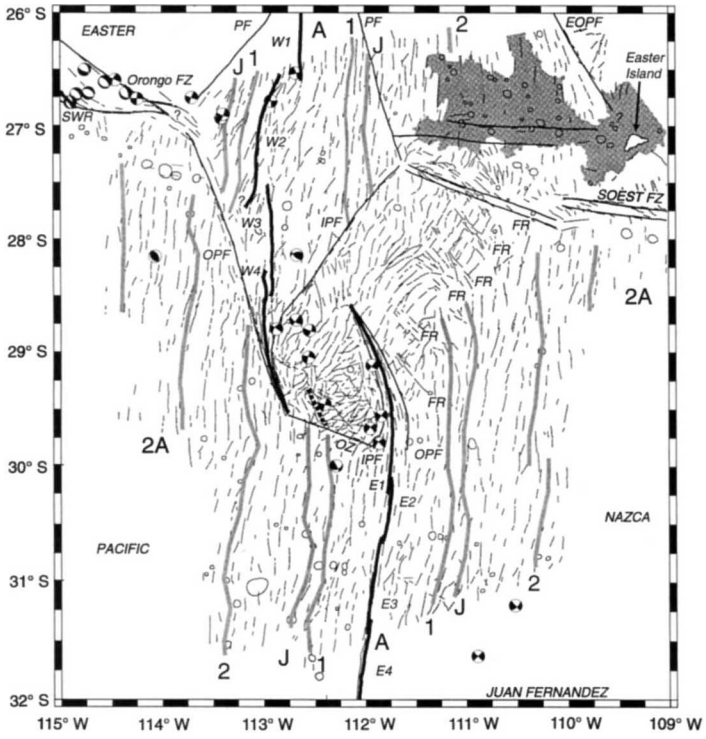

FIG. 3 Simplified tectonic interpretation based primarily on GLORI-B sidescan sonar (Fig. 2*b*) and SeaBeam 2000 bathymetry (see Fig. 2*a*). Heavy lines show active plate boundaries, the heavy dashed line is a new rift graben, medium lines are pseudofaults (PF) and fracture zones (FZ), and light lines are representative fault scarps showing sea-floor structural fabric. The zone of lithosphere transferred from the Pacific to the Nazca plate is marked by northeast-trending fabric extending northeast from the 29° S overlap zone. Cross-cutting structures in this zone are failed rifts (FR), and OZ is the southern boundary of the overlap zone. Circular structures are volcanoes, the shaded area (top right) is the Ahu volcanic field, and beachballs are focal mechanisms (from the Harvard centroid moment tensor catalogue on the Internet (http://tempo.harvard.edu/CMT.html), and from ref. 24 for locations near the overlap zone). Lightly shaded lines are isochrons from magnetic anomalies (1 is Brunhes/Matuyama reversal, J is Jaramillo event). SWR is the Southwest rift of the Easter microplate and E1–E4 and W1–W4 are the East and West segments of the inter-microplate ridge system. OPF and IPF are the outer and inner pseudofaults of the duelling propagators, EOPF is the outer pseudofault of the initial Easter microplate propagator.

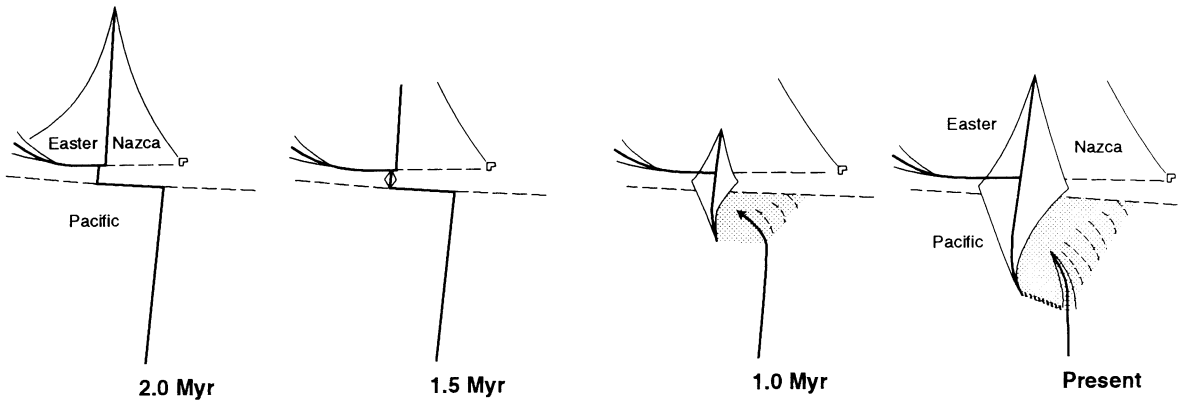

FIG. 4 Schematic evolution from transform fault to duelling propagators to possible proto-microplate. Heavy lines are active plate boundaries, long dashed lines are fracture zones, short dashed lines are failed rifts. Light lines are V-shaped pseudofault wakes of dominant propagators, arrows show briefly active duelling propagators. The northward propagator with outer pseudofault extending to Easter Island, shown schematically at 2 Myr (from ref. 3), is the one which seems to have initiated Easter microplate formation[1–3], probably driven by the magma pulse that formed Easter Island. Shading shows transferred lithosphere. Details of this evolution will be presented elsewhere (J.K. and R.N.H., manuscript in preparation).

microplate, the 120-km diameter requires[7] a rotation rate of 72° per Myr to match the regional spreading rates. The close fit of observed and predicted structures based on the propagating rift equations thus indicates at most a very brief period of additional microplate rotation. However, there are notable differences between the fossil and present overlap zones. No analogue of the NNW-trending rift graben, the northwest-trending scarp to the east, or the transform-like southern boundary in the present overlap zone is observed in the fossil overlap zone. This suggests that the tectonic behaviour has changed recently. One possibility is that a new microplate may be beginning to form here. A small rift graben adjacent to a transform boundary is also seen within the proposed Wilkes "nannoplate"[31], although grabens in migrating extensional relay zones have also been proposed to be characteristic of propagating rift systems[32].

Although there may have been a recent brief attempt to begin to rotate as a mostly rigid microplate, the successful evolution of this duelling propagator system into an edge-driven microplate[7] would require the eventual formation of a northern boundary as well. The width of this overlap zone (~120 km) is slightly smaller than those of the pervasively deformed cores of the Easter[2] and Juan Fernandez[5] microplates (~130–140 km), suggesting that this is about the scale at which pervasive sea-floor shearing of the overlap zone is no longer possible, the lithosphere stops deforming and begins to rotate as a rigid microplate[3,6,7,9,18]. The aspect ratios of the deformed cores of the microplates are ~3:1 (Easter) and ~2:1 (Juan Fernandez), suggesting that for this overlap zone to evolve into a similar microplate there would have to be a linkage event resulting from very rapid propagation that would double or triple the overlap length. □

Received 4 May; accepted 25 September 1995.

1. Hey, R. N. *et al. Nature* **317,** 320–325 (1985).
2. Searle, R. C. *et al. Nature* **341,** 701–705 (1989).
3. Naar, D. F. & Hey, R. N. *J. geophys. Res.* **96,** 7961–7993 (1991).
4. Francheteau, J., Yelles-Chaouche, A. & Craig, H. *Earth planet. Sci. Lett.* **86,** 253–268 (1987).
5. Larson, R. L. *et al. Nature* **356,** 571–576 (1992).
6. Searle, R. C., Bird, R. T., Rusby, R. I. & Naar, D. F. *J. geol. Soc. Lond.* **150,** 965–976 (1993).
7. Schouten, H., Klitgord, K. D. & Gallo, D. G. *J. geophys. Res.* **98,** 6689–6701 (1993).
8. Gallo, D. G. & Fox, P. J. (abstr.) *Eos* **63,** 446 (1982).
9. Engeln, J. F. & Stein, S. *Earth planet. Sci. Lett.* **68,** 259–270 (1984).
10. Bird, R. T. & Naar, D. F. *Geology* **22,** 987–990 (1994).
11. Hey, R. N. *Earth planet. Sci. Lett.* **37,** 321–325 (1977).
12. Schilling, J.-G., Sigurdsson, H., Davis, A. N. & Hey, R. N. *Nature* **317,** 325–331 (1985).
13. Hey, R. N., Duennebier, F. K. & Morgan, W. J. *J. geophys. Res.* **85,** 3647–3658 (1980).
14. McKenzie, D. P. *Earth planet. Sci. Lett.* **77,** 176–186 (1986).
15. Cormier, M.-H. & Macdonald, K. C. *J. geophys. Res.* **99,** 543–564 (1994).
16. Naar, D. F. & Hey, R. N. in *Evolution of Mid Ocean Ridges* (ed. Sinton, J. M.) 9–30 (American Geophysical Union, Washington DC, 1989).
17. Shackleton, N. J., Berger, A. & Peltier, W. R. *Trans. R. Soc. Edinb.* **81,** 251–261 (1990).
18. Klaus, A., Icay, W., Naar, D. F. & Hey, R. N. *J. geophys. Res.* **96,** 9985–9998 (1991).
19. Johnson, H. P. *et al. J. geophys. Res.* **88,** 2297–2315 (1983).
20. Macdonald, K. C., Haymon, R. M., Miller, S. P., Sempere, J.-C. & Fox, P. J. *J. geophys. Res.* **93,** 2875–2898 (1988).
21. Lonsdale, P. *J. geophys. Res.* **84,** 713–743 (1989).
22. Wilson, D. S. *Earth planet. Sci. Lett.* **96,** 384–392 (1990).
23. Kleinrock, M. C. & Hey, R. N. *J. geophys. Res.* **94,** 13859–13878 (1989).
24. Wetzel, L. R., Wiens, D. A. & Kleinrock, M. C. *Nature* **362,** 235–237 (1989).
25. Korenaga, J. *J. geophys. Res.* **100,** 365–378 (1995).
26. Hey, R. N., Kleinrock, M. C., Miller, S. P., Atwater, T. M. & Searle, R. C. *J. geophys. Res.* **91,** 3369–3393 (1986).
27. Phipps Morgan, J. & Parmentier, E. M. *J. geophys. Res.* **90,** 8603–8612 (1985).
28. Naar, D. F. & Hey, R. N. *Geology* **17,** 420–422 (1989).
29. Smith, W. H. F. & Sandwell, D. T. *J. geophys. Res.* **99,** 21803–21824 (1994).
30. Scheirer, D. S. & Macdonald, K. C. *J. geophys. Res.* **98,** 7871–7885 (1993).
31. Goff, J. A., Fornari, D. J., Cochran, J. R., Keeley, C. & Malinverno, A. *Geology* **21,** 623–626 (1993).
32. Kleinrock, M. C., Searle, R. C. & Hey, R. N. *J. geophys. Res.* **94,** 13839–13858 (1989).

ACKNOWLEDGEMENTS. We thank the captain and crew of the RV *Melville*, and J. Campbell and R. Beale of the GLORIA group for their help, the USGS for the use of their GLORIA/B system, and the government of Chile for permission to survey. We thank D. Wilson and J. Goff for reviews, D. McKenzie, R. Searle, J. Francheteau, B. Taylor, K. Macdonald, J. Phipps Morgan, P. Tapponnier, I. Manighetti and R. Armijo for discussions, and L. Norby, C. Inouye, T. Duennebier, and N. Hulbirt for assistance. This work was supported by the US NSF.

Elasticity of forsterite to 16 GPa and the composition of the upper mantle

Thomas S. Duffy*, Chang-sheng Zha, Robert T. Downs, Ho-kwang Mao & Russell J. Hemley

Geophysical Laboratory and Center for High-Pressure Research, Carnegie Institution of Washington, 5251 Broad Branch Road, NW, Washington DC 20015, USA

NEARLY 60 years ago, Bernal[1] proposed that a polymorphic phase transformation in olivine might be responsible for the seismic velocity discontinuity near 410 km depth in the mantle. Phase equilibria experiments[2,3] have since shown that the olivine (α) to wadsleyite (β) transition in $(Mg,Fe)_2SiO_4$ occurs at the appropriate pressure (13.8 GPa) under mantle conditions. Comparison of laboratory measurements of the acoustic velocity contrast in the α–β system to the magnitude of the seismically observed discontinuity at 410 km provides a way to constrain the olivine content of the mantle at this depth. Here we report measurements of the

* Present address: Consortium for Advanced Radiation Sources, The University of Chicago, 5640 South Ellis, Chicago, Illinois 60637, USA